J|A|C|S ARTICLES

Published on Web 08/11/2010

Hexagonal Superlattice of Chiral Conducting Polymers Self-Assembled by Mimicking β-Sheet Proteins with Anisotropic Electrical Transport

Yong Yan,[†,‡] Rui Wang,[†,‡] Xiaohui Qiu,[†] and Zhixiang Wei*[,†]

National Center for Nanoscience and Technology, Beijing 100190, P. R. China, and Graduate School of the Chinese Academy of Sciences, Beijing 100039, P. R. China

Received April 29, 2010; E-mail: weizx@nanoctr.cn

Abstract: An ordered superlattice self-assembled from monodispersed nanostructures can exhibit collective effects of its individual building blocks, a desirable property that gives rise to potential applications. However, no general method for the direct fabrication of superstructures yet exists, especially for superlattices that start from rational-designed functional molecules. Noncovalent interactions are widely used for the self-assembly of biomolecules in nature, such as various superstructures of proteins. Instead of using hydrogen bonds as driving force for the self-assembly of β-sheet structures of peptides, $\pi-\pi$ stacking interactions were used in this study to self-assemble conducting polyaniline (PANI) nanostructures and superstructures. Monodispersed crystalline PANI nanorices were prepared by using homochiral PANI as building blocks; these nanorices can further self-assemble into hexagonal microplates aligned shoulder to shoulder. PANI molecules were organized into nanorices via single-handed helical $\pi-\pi$ stacking, in which the molecular plane was normal to the long axis of the nanorices. Electrical transport measurements showed the anisotropic characteristics of self-assembled nanorices and their superstructures, which were due to the directional transport barrier in the nanorices and the structural defects at the interfaces between neighboring nanorices. As chiral PANI and peptides have similar self-assembly behaviors, the method used in this study is greatly expected to be applicable to other chemical and biochemical building blocks.

Introduction

Functional nanostructures that self-assemble into ordered superstructures arouse great attention due to their unique properties and device-oriented applications.[1−3] Compared to disordered aggregates, ordered superstructures show the collective effects of the coupling of the optical and electronic properties of neighboring nanostructured building blocks.[4,5] Well-defined, one-dimensional (1D), two-dimensional (2D), and even three-dimensional (3D) ordering architectures with geometric controls and functionality have recently been realized.[6−9] However, producing these ordered structures require either special techniques, such as external field induction, microfluidic channel control, and soft lithography, or special building blocks, such as nanostructures that selectively bind with ligands and biorecognitive counterparts.[10−23] Given the diversity and complexity of the existing procedures, a simple, general method for arranging individual nanostructures into ordered superstructures with collective functions is highly desirable, as this facilitates the study of the potential applications of nanostructures.

Understanding molecular interactions and the assembly mechanisms of biological molecules is a crucial factor in designing nanoscale functional materials. Many fascinating nanostructures and superstructures, for example, have recently

[†] National Center for Nanoscience and Technology.
[‡] Graduate School of the Chinese Academy of Sciences.

(1) Whitesides, G. M.; Grzybowski, B. *Science* **2001**, *295*, 2418.
(2) Liu, W.; Lieber, C. M. *Nat. Mater.* **2007**, *6*, 841.
(3) Melosh, N. A.; Boukai, A.; Diana, F.; Gerardot, B.; Badolato, A.; Petroff, P. M.; Heath, J. R. *Science* **2003**, *300*, 112.
(4) Ghosh, S. K.; Pal, T. *Chem. Rev.* **2007**, *107*, 4797.
(5) Pileni, M. P. *J. Phys. Chem. B* **2001**, *105*, 3358.
(6) Xia, Y.; Yang, P.; Sun, Y.; Wu, Y.; Mayers, B.; Gates, B.; Yin, Y.; Kim, F.; Yan, H. *Adv. Mater.* **2003**, *15*, 353.
(7) Tang, Z.; Kotov, N. M.; Giersig, M. *Science* **2002**, *297*, 237.
(8) Zhao, N.; Liu, K.; Greener, J.; Nie, Z.; Kumacheva, E. *Nano Lett.* **2009**, *9*, 3077.
(9) Redl, F. X.; Cho, K.-S.; Murray, C. B.; O'Brien, S. *Nature* **2003**, *423*, 968.
(10) Ryan, K. M.; Mastroianni, A.; Stancil, K A.; Liu, H.; Alivisatos, A. P. *Nano Lett.* **2006**, *6*, 1479.
(11) Huang, Y.; Duan, X.; Wei, Q.; Lieber, C. M. *Science* **2001**, *291*, 630.
(12) Tao, A.; Kim, F.; Hess, C.; Goldberger, J.; He, R.; Sun, Y.; Xia, Y.; Yang, P. *Nano Lett.* **2003**, *3*, 1229.
(13) Huang, J.; Kim, F.; Tao, A. R.; Connor, S.; Yang, P. *Nat. Mater.* **2005**, *4*, 896.
(14) Hochbaum, A. I.; Fan, R.; He, R.; Yang, P. *Nano Lett.* **2005**, *5*, 457.
(15) Park, S.; Lee, D. H.; Xu, J.; Kim, B.; Hong, S. W.; Jeong, U.; Xu, T.; Russell, T. P. *Science* **2009**, *323*, 1030.
(16) Tang, Z.; Zhang, Z.; Wang, Y.; Glotzer, S. C.; Kotov, N. A. *Science* **2006**, *314*, 274.
(17) Guiton, B. S.; Davies, P. K. *Nat. Mater.* **2007**, *6*, 586.
(18) Nie, Z.; Fava, D.; Kumacheva, E.; Zou, S.; Walker, G. C.; Rubinstein, M. *Nat. Mater.* **2007**, *6*, 609.
(19) Shevchenko, E. V.; Talapin, D. V.; Kotov, N. A.; O'Brien, S.; Murray, C. B. *Nature* **2006**, *439*, 55.
(20) Bigioni, T. P.; Lin, X.; Nguyen, T. T.; Corwin, E. I.; Witten, T. A.; Jaeger, H. M. *Nat. Mater.* **2006**, *5*, 265.
(21) Lin, C.; Ke, Y.; Liu, Y.; Mertig, M.; Gu, J.; Yan, H. *Angew. Chem., Int. Ed.* **2007**, *46*, 6089.
(22) Aldaye, F. A.; Palmer, A. L.; Sleiman, H. F. *Science* **2008**, *321*, 1795.
(23) Caswell, K. K.; Wilson, J. N.; Bunz, U. H. F.; Murphy, C. J. *J. Am. Chem. Soc.* **2006**, *128*, 13084.

10.1021/ja1036447

been realized using DNA and peptides as building blocks via a bottom-up process.[24−29] The β-sheet, in which peptides are connected laterally by hydrogen bonds,[30,31] is a common structural form for the self-assembly of various biological nanostructures. Aside from hydrogen bonds, $\pi-\pi$ stacking interactions can be utilized as the basic driving force for self-assembling nanostructures of conjugated molecules.[32] As is commonly known, both hydrogen bonding and $\pi-\pi$ stacking interactions are directional interactions; therefore, using synthetic conjugated molecules, especially building blocks with chiral structures and conformation, to self-assemble into ordered nanostructures and superstructures by mimicking the assembly behavior of biomolecules is of great importance for designing novel, functional nanomaterials.

Conducting polyaniline (PANI) is a typical conjugated, multifunctional polymer; it has been widely used in electrically, optically, and chemically active materials and devices.[33−35] Various nanostructures of PANI, including induced helical nanofibers, have been produced by either template or template-free methods.[36−43] However, good crystalline PANI nanostructures, especially those with anisotropic architectures and functions,[44] have rarely been prepared. Furthermore, preparation of well-defined topological superstructures from PANI nanostructures still remains a scientific challenge. In this study, $\pi-\pi$ stacking interactions were used to guide the self-assembly of conducting PANI by mimicking the self-assembly process of β-sheet structures driven by hydrogen bonding. Monodispersed nanorices of PANI were prepared using chiral PANI molecules as building blocks. These monodispersed nanorices further assembled into ordered hexagonal microplates aligned shoulder to shoulder by delicately controlling the good-solvent-to-poor-solvent ratio.

Experimental Section

Synthesis of Chiral PANI Solutions. Aniline monomers and solvents were distilled prior to use. 2,3-Dichloro-5,6-dicyano-1,4-benzoquione (DDQ) and D- or L-camphorsulfonic acid (CSA) were used as received without further treatment. A typical PANI polymerization process was performed as follows: D-CSA was first dissolved in 5.0 mL of chloroform. Aniline (56.9 μL, 0.625 mmol) and a small amount of the oligomer *N*-phenyl-*p*-phenylenediamine (1/500 molar ratio of aniline) were then added to the solution. The solution was shaken vigorously for full dissolution and left undisturbed for 1 h. To this was added one portion of DDQ (142 mg, 0.625 mmol) predissolved in 1.675 mL of THF. The reaction mixture was vigorously shaken for 5 min to achieve full dispersion and was left to stand at 25 °C for 12 h to complete polymerization. The as-prepared PANI solution was then diluted in a good solvent (a mixture of THF and $CHCl_3$ at a volume ratio of 1/3) for CD and UV−vis measurements.

Self-Assembly of Helical Nanowires, Nanorices, and Ordered Hexagonal Microplates. As-prepared chiral PANI (0.1 mL) was first diluted in different volumes of good solvent. Poor solvent (methanol) was then added to these dilutions in different good-solvent-to-poor-solvent ([G]/[P]) ratios; the combined volume of the two solvents, however, was kept constant at 8.0 mL. The mixtures were vigorously shaken for 5 min and left to stand for 24 h for self-assembly, by which time, nanostructures and superstructures had already formed and deposited at the bottom of the vials. The clear, upper portion in each vial was extracted and the nanostructures and superstructures were washed several times with methanol; the lower portion was drop-cast on either a silicon wafer or a carbon-coated copper grid for SEM, TEM, and SAED characterization. Dried samples representing each of the [G]/[P] ratios left in dynamic vacuum for 24 h at room temperature were used for XRD characterization. For the characterization of circular dichroism (CD) and UV−vis spectra, the as-self-assembled samples were redispersed by hand shaking and direct for test without further purification.

Morphology and Structure Characterizations. The morphologies of the resulting helical nanostructures were examined by SEM (S-4800, Hitachi, Japan) and TEM (Tecnai G^2 F20 U-TWIN, FEI Co., USA). CD spectra were characterized using Jasco J810 equipment and UV−vis absorption spectra were recorded using a PerkinElmer Lambda 950 instrument. Electrical transport was conducted by an AFM (Dimension 3100, Veeco, USA). The crystalline structures were measured by XRD (D/max-rA 12 kW).

Electrical Transport Measurement of Nanorices and Ordered Hexagonal Microplates. Anisotropic electrical transport was measured by a conducting probe AFM, with the tip serving as one electrode and sputtered Au film on a silicon substrate as the other. The electrical conductivities in the normal and parallel directions were obtained by locating the conductive probe at the top of the hexagonal sheet and the side of the single nanorice, respectively. The $I-V$ characteristics were recorded using a Keithley 4200-SCS semiconductor parameter analyzer. For the in-plane direction, the microplate was drop-cast on interdigitated, neighboring gold microstripes serving as electrodes and conducted by a micromanipulator 6150 probe station in a clean and shielded box in ambient laboratory environment at room temperature. The $I-V$ characteristics of this direction were also recorded using the Keithley 4200-SCS semiconductor parameter analyzer.

Results and Discussion

The preparation of PANI nanostructures and superstructures first required the preparation of unique building blocks of conducting PANI with a predominantly one-handed helical chain conformation in good solvent via the induction of CSA. As-prepared chiral PANI solution was then diluted in good solvent, followed by the addition of poor solvent (methanol) to self-assemble PANI nanostructures and superstructures. Interestingly, slightly change in the [G]/[P] ratio can shift PANI nanostructure arrangement from nanorices to shoulder-to-shoulder hexagonal microplates and finally to disordered nanowires.

A slow self-assembly process produced monodispersed nanorices at a relatively high [G]/[P] ratio (e.g., 50/50 in

(24) Sharma, J.; Chhabra, R.; Cheng, A.; Brownell, J.; Liu, Y.; Yan, H. *Science* **2009**, *323*, 112.
(25) Douglas, S. M.; Dietz, H.; Liedl, T.; Högberg, B.; Graf, F.; Shih, W. M. *Nature* **2009**, *459*, 414.
(26) Zhao, X.; Zhang, S. *Macromol. Biosci.* **2007**, *7*, 13.
(27) Dietz, H.; Douglas, S. M.; Shih, W. M. *Science* **2009**, *325*, 725.
(28) Hamley, I. W. *Angew. Chem., Int. Ed.* **2007**, *46*, 8128.
(29) Scanlon, S.; Aggeli, A. *Nanotoday* **2008**, *3*, 22.
(30) Ulijn, R. V.; Smith, A. M. *Chem. Soc. Rev.* **2008**, *37*, 664.
(31) Jahn, T. R.; Makin, O. S.; Morris, K. L.; Marshall, K. E.; Tian, P.; Sikorski, P.; Serpell, L. C. *J. Mol. Biol.* **2010**, *395*, 717.
(32) Hoeben, F. J. M.; Jonkheijm, P.; Meijer, E. W.; Schenning, A. *Chem. Rev.* **2005**, *105*, 1491.
(33) Huang, J.; Virji, S.; Weiller, B. H.; Kaner, R. B. *J. Am. Chem. Soc.* **2003**, *125*, 314.
(34) Wan, M.; Li, J.; Li, S. *Polym. Adv. Technol.* **2001**, *12*, 651.
(35) Chang, H.; Yuan, Y.; Shi, N.; Guan, Y. *Anal. Chem.* **2007**, *79*, 5111.
(36) Martin, C. R. *Acc. Chem. Res.* **1995**, *28*, 61.
(37) Lee, K.; Cho, S.; Park, S. H.; Heeger, A. J.; Lee, C.; Lee, S. *Nature* **2006**, *441*, 65.
(38) Huang, J.; Kaner, R. B. *J. Am. Chem. Soc.* **2004**, *126*, 851.
(39) Chiou, N. R.; Lu, C.; Guan, J.; Lee, L. J.; Epstein, A. J. *Nat. Nanotechnol.* **2007**, *2*, 354.
(40) Wei, Z.; Zhang, Z.; Wan, M. *Langmuir* **2002**, *18*, 917.
(41) Majidi, M. R.; Kane-Maguire, L. A. P.; Wallace, G. G. *Polymer* **1995**, *36*, 3597.
(42) Li, W. G.; Wang, H. L. *J. Am. Chem. Soc.* **2004**, *126*, 2278.
(43) Yan, Y.; Yu, Z.; Huang, Y. W.; Yuan, W. X.; Wei, Z. X. *Adv. Mater.* **2007**, *19*, 3353.
(44) Nuraje, N.; Su, K.; Yang, N. I.; Matsui, H. *ACS Nano* **2008**, *2*, 502.

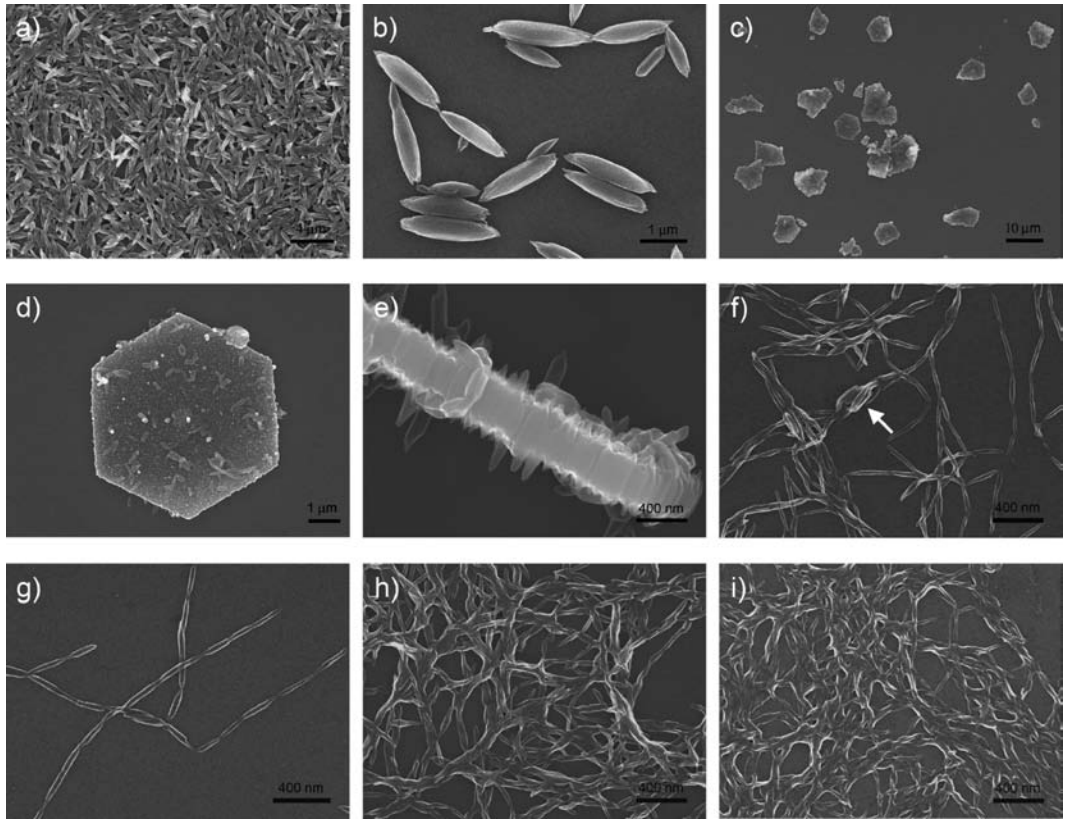

Figure 1. SEM images of chiral PANI nanorices, ordered hexagonal microplates, and nanowires. Panels a and b show the SEM images of nanorices at low and high magnifications obtained at a [G]/[P] ratio of 50/50. Panels c and d show the images of superstructure microplates observed at low and high magnification obtained at a [G]/[P] ratio of 40/60. Panel e shows the side view of a microplate; nanorices arranged shoulder to shoulder are clearly observed. Panels f and g show the SEM images of necklace-like nanowires obtained at a [G]/[P] ratio of 30/70. Panel f indicates that although some nanorice superstructures are arranged shoulder to shoulder, such as shown by the bright arrow, most nanorices are connected along the long axis direction and form necklace-like architectures. Panel g is a relatively sparse area, which shows much clearer necklace-like arrangements. Panels h and i show PANI nanowires obtained with a fast self-assembly process at [G]/[P] ratios of 20/80 and 10/90, respectively. The tendency of the nanorices to transform into helical nanowires can be observed.

Figure 1a,b). This study found that increasing the proportion of good solvent slows deposition rate of the nanostructures and superstructures. The self-assembly process can therefore be described as "slow" or "fast", depending on how quick the nanostructures and superstructures deposit at the bottom of the vial. When the [G]/[P] ratio is decreased to 40/60, PANI nanorices self-assembled into hexagonal superstructured microplates (Figure 1c−e). A low-magnification image (Figure 1c) indicates that the microplates were spread everywhere, and even though only a few ordered hexagonal microplates are seen, the angles and sides of the ordered hexagonal microplates from the ruptures can be clearly recognized. The ruptures formed because the superstructure formation process was not complete and external disturbances broke the microplates during either the superstructure formation process or the postprocessing procedure. The side view of one microplate (Figure 1e) shows the shoulder-to-shoulder arrangement of nanorices in their superstructures. Further decreases in the [G]/[P] ratio produced PANI nanowires with a faster self-assembly process. In summary, transformation from necklace-like nanorices to helical nanowires tended to occur with a decrease in the [G]/[P] ratio, specifically from 30/70 in Figure 1f,g, to 20/80 in Figure 1h, and finally to 10/90 in Figure 1i. Although some superstructures with shoulder-to-shoulder arrangements of monodispersed nanorices were found (Figure 1f, bright arrow), most nanorices were connected along the long axis direction to form necklace-like architectures and, finally, helical nanowires.

The formation of superstructures is ascribed to the delicate control of the Brownian motion and van der Waals forces among the PANI molecules and their self-assembled nanostructures. With a high proportion of good solvent, the Brownian motion of the PANI molecules dominated, resulting in a dynamic equilibrium between individual molecules and their small aggregates. With the addition of poor solvent, van der Waals forces, especially $\pi-\pi$ stacking interactions between the PANI molecules, suppressed the solvent effect. Monodispersed nanorices (Figure 1a,b) were obtained as a result of PANI aggregation along the $\pi-\pi$ stacking directions. With further increases in the proportion of the poor solvent, the interactions among the PANI nanorices overcame the Brownian motion of the nanoparticles. As a result, the PANI nanorices self-organized shoulder to shoulder to form closely packed hexagonal microplates (Figure 1c−e) and also decreasing the diameters of individual nanorices. Increasing the proportion of the poor solvent, therefore, resulted in a faster self-assembly process. Moreover, due to strong $\pi-\pi$ stacking interactions, nanorices connected with each other and assumed a necklace-like configuration and ultimately formed helical nanowires (Figure 1f−i). Hence, by adjusting the [G]/[P] ratio, the morphologies of nanostructures and superstructures can be manipulated. Since the Brownian

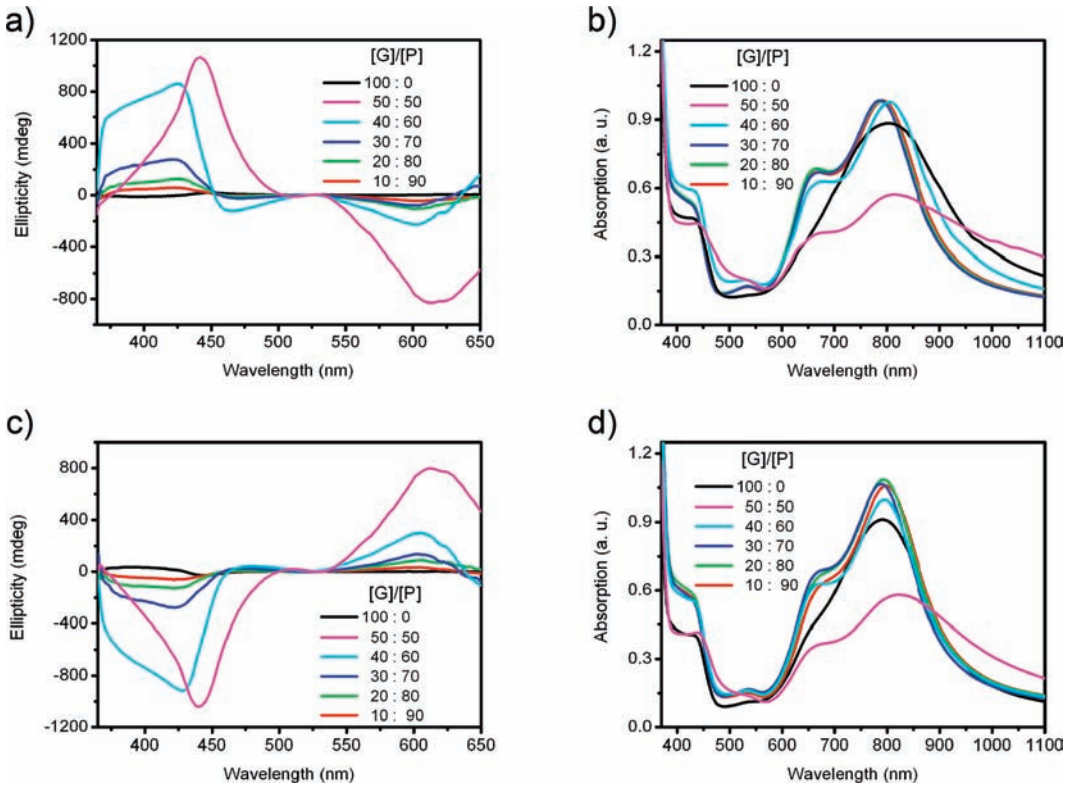

Figure 2. CD and UV−vis spectra of the chiral PANI solutions, nanostructures, and superstructures. Panels a and b are induced by the D-enantiomers of CSA, whereas panels c and d are induced by the L-enantiomers of CSA. Interestingly, the CD spectra of the PANI nanostructures and superstructures are the inverse of those of PANI in solution.

motion and van der Waals forces are the basic factors in the self-assembly process, the method is highly expected to be applicable to other functional systems.

One of the unique characteristics of self-assembled superstructures is that PANI molecular building blocks possess a predominantly one-handed helical conformation. In this study, PANI doped by D-CSA in good solvent showed a bisignated CD signal with a negative CD band at ca. 400 nm and a positive band at ca. 450 nm (Figure 2a), which corresponded to the peak splitting at 440 nm in UV−vis spectra (Figure 2b).[45] All nanostructures and superstructures showed intense, positive CD bands at 400−450 nm which were inverse to those of the PANI solutions. The inversion of the CD signal indicates that the stacking direction of the PANI plane was normal to the long axis of the nanorices and nanowires.[46] The ellipticity of the nanorice and superstructure microplates was stronger than that of the nanowires, indicating a higher degree of helical stacking due to a slower self-assembly process. The negative bands at 610 nm in the CD spectra of nanorices and microplates resulted from the partial dedoping of PANI and corresponded to the absorption peak at 660 nm in UV−vis spectra.

On the other hand, L-CSA-doped PANI registered mirror images of D-CSA doped PANI in the CD spectra. Their UV−vis spectra, however, were almost identical (Figures 2b,d), which further proved that chiral PANI is induced by a chiral dopant. The helical conformation and stacking of PANI molecules played an important role in the formation of the hexagonal superlattice, which will be discussed vide infra.

For PANI nanostructures and superstructures, the appearance of a dominant absorption band at ca. 800 nm in UV−vis spectra (Figure 2b,d) suggests that the PANI molecules were almost in the doping state. This is also indicated by the green color of the solutions both before and after assembly. On the other hand, the appearance of the weak shoulder peak at ca. 660 nm in the UV−vis spectra (Figures 2b,d) indicate that PANI nanostructures and superstructures were only partially dedoped because the solution had a low concentration of CSA and the solvent effect.

Partial dedoping PANI leads to a decrease in its conductivity. We therefore investigated the absorption spectra of PANI in films and attempted to redope PANI nanostructures and superstructures in the solid state. The UV−vis spectra of the PANI films were recorded by drop-casting them onto quartz plates at different [G]/[P] ratios. PANI films that were drop-cast on plates with 100% good solvent ([G]/[P] = 100/0) showed an absorption hand at ca. 790 nm, but none in the infrared (IR) region (Figure 3a), indicating that the PANI molecules were in a conducting state with a coiled-like conformation.[47,48] When methanol was added ([G]/[P] = 40/60 or 50/50), an IR absorption band higher than 800 nm emerged. We hypothesize that methanol played a role similar to that of phenols, as mentioned in literature, changing the conformation of PANI from coil-like to extended coil.[47,48] On the other hand, shoulder peaks at ca. 650 nm became weaker but still existed, indicating

(45) MacDiarmid, A. G.; Epstein, A. J. *Synth. Met.* **1995**, *69*, 85.
(46) Tabei, J.; Nomura, R.; Shiotsuki, M.; Sanda, F.; Masuda, T. *Macromol. Chem. Phys.* **2005**, *206*, 323.
(47) Xia, Y.; Wiesinger, J. M.; MacDiarmid, A. G. *Chem. Mater.* **1995**, *7*, 443.
(48) Tigelaar, D. M.; Lee, W.; Bates, K. A.; Saprigin, A.; Prigodin, V. N.; Cao, X.; Nafie, L. A.; Platz, M. S.; Epstein, A. J. *Chem. Mater.* **2002**, *14*, 1430.

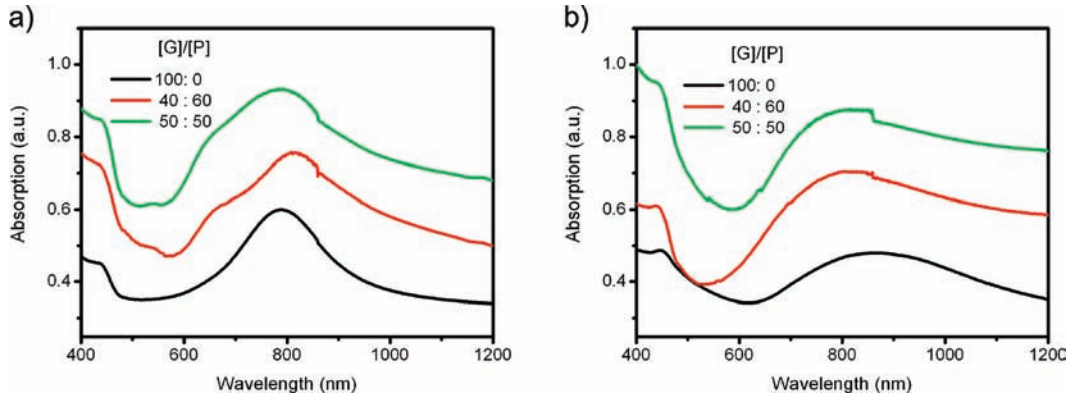

Figure 3. UV−vis spectra of PANI films. Panel a shows the UV−vis spectra of PANI superstructure films obtained by drop-casting on a quartz plate with different [G]/[P] ratios. Panel b shows the UV−vis spectra of the above films after immersion in 0.2 M CSA aqueous solution and drying in ambient conditions.

that the dedoping of PANI cannot be fully repaired after removing the solvent. The film was then immersed in 0.2 M CSA aqueous solution for 1 h. PANI in the film that was drop-cast in good solvent kept its coil-like conformation; however, the absorption band red-shifted. Therefore, PANI nanostructures and superstructures obtained at different [G]/[P] ratios can be fully redoped and exist in an extended coil conformation, which facilitates their charge carrier transport.

The arrangement of PANI molecules in their nanostructures and superstructures were subsequently characterized by TEM, SAED, and XRD, as shown in Figure 4. SAED and XRD revealed chiral PANI molecules to be long-range-ordered in the nanorices and hexagonal microplates. Diffused reflections of single nanorices (Figure 4b) correspond to a *d* spacing of ca. 3.5 Å and result from the $\pi-\pi$ stacking of planar PANI molecules along the long axis of the nanorice. Rather sharp reflections corresponding to a *d* spacing of ca. 6.0 Å possibly originate from the arrangement of CSA molecules setting between neighboring PANI chains. The sharp reflections in the SAED pattern corresponding to a *d* spacing of 10 Å could be assigned to the high-ordered reflections corresponding to the distance between PANI chains.[49,50] In fact, this packing means is very common in biological species such as the β-pleated sheet of proteins,[30,31] in which the basic unit of chiral peptides is normal to the direction of their 1D nanostructure, which is very similar to the chiral PANI in the nanorice. However, the driving force behind the 1D nanostructure of peptides is hydrogen bonding instead of the $\pi-\pi$ interactions observed with PANI. Overall, the building blocks of chiral PANI are quite similar to random-coiled peptides in solution, and the nanorice is an analog of β-sheet assemblies of peptides formed by different noncovalent interactions.

To further investigate the arrangement direction of PANI molecules normal to that of $\pi-\pi$ stacking, SAED was carried out with the electron beam direction normal to the microplate plane. Interestingly, both reflections corresponding to *d* spacings of 6.0 and 10 Å in the SAED pattern of nanorices showed hexagonal symmetry along the direction normal to the microplate plane. Hexagonal symmetry was attributed to the helical stacking of PANI molecules, in which the 2D columnar phase reported in the literature transformed to a 2D hexagonal phase.[51] This hexagonal symmetry was transcribed to higher levels in the self-assembly process; hence, hexagonal microplates were finally obtained. The XRD spectra of both nanorices and hexagonal microplates were nearly identical, with three characteristics peaks at ca. 9°, 14°, and 25°, fitting very well with *d* spacings of 10, 6.0, and 3.5 Å in the SAED patterns, respectively. Based on the results of SAED and XRD, a 1D structural model was proposed for the PANI nanorice (Figure 4f) in which PANI molecules are arranged normal to the nanorice axial direction and stacked in a helical manner.

Chiral PANI molecules are arranged normal to the long axis of the nanorice. As a consequence, anisotropic electrical conductivity was expected due to the different transport mechanism between the $\pi-\pi$ stacking direction and polymer main chain direction. Measurement of conductivities along different directions is schematically shown in Figure 5a−c. To study the electrical transport characteristics of the $\pi-\pi$ stacking direction, the microplate was first drop cast on a silicon substrate with sputtered gold film, and the conducting probe of AFM was used as the top electrode. For the normal direction, the AFM probe was directly loaded onto a disassociated nanorice; for the in-plane direction, the microplate was drop-cast on interdigitated gold electrodes. The AFM images of the microplate and the nanorice are shown in Figure 5d,e, respectively; the SEM image showing microplate bridging between two interdigitated gold electrodes is shown in Figure 5f. All of the $I-V$ curves are linear and symmetrical, which indicates that contact resistance is negligible, that is, the contact was ohmic in nature. $I-V$ results showed that the $\pi-\pi$ stacking direction had the highest conductivity (16 S/cm), much higher than the conductivity of the direction normal to the nanorice axis (0.94 S/cm). On the other hand, the in-plane direction of the microplates shows the lowest conductivity (0.030 S/cm).

The anisotropic conductivity of the microplates is originated from the anisotropic arrangement of the PANI molecules. For the normal direction of the microplates, charge carriers are transported between interchains via the $\pi-\pi$ orbital overlapping of PANI chains. Due to the good crystallinity of nanorices, this direction has the highest

(49) Łużny, W.; Samuelsen, E. J.; Djurado, D.; Nicolau, Y. F. *Synth. Met.* **1997**, *90*, 19.
(50) Pouget, J. P.; Hsu, C. H.; Mac Diarmid, A. G.; Epstein, A. J. *Synth. Met.* **1995**, *69*, 119.
(51) Wurthner, F.; Thalacker, C.; Diele, S.; Tschierske, C. *Chem.—Eur. J.* **2001**, *7*, 2245.

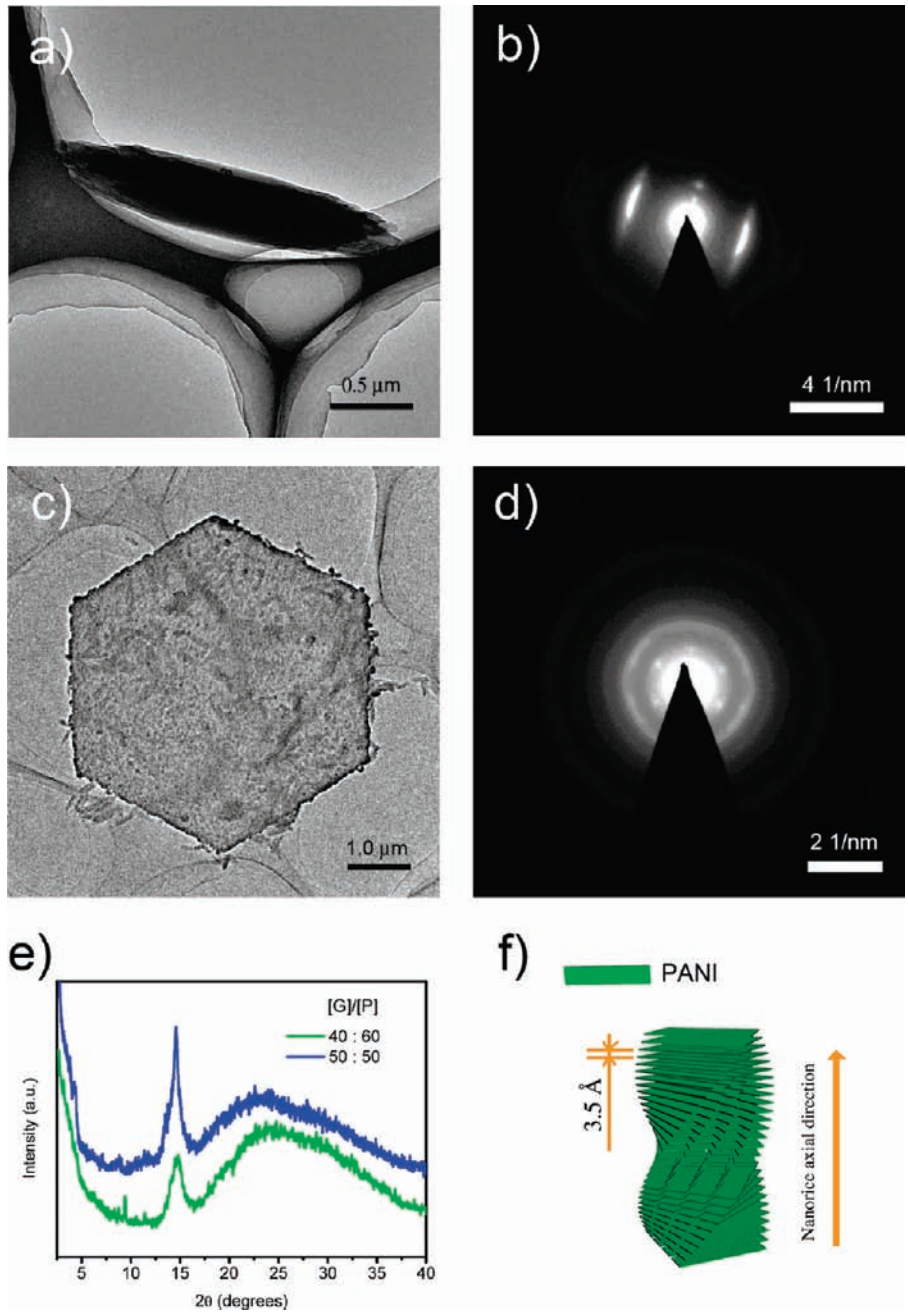

Figure 4. TEM images, SAED patterns, and XRD spectra of chiral PANI nanorices and ordered hexagonal microplates. Panel a shows the TEM image and panel b shows the SAED pattern of a nanorice with well crystallization. Panel c shows the TEM image, and panel d shows the SAED pattern of microplates with the same hexagonal conformations. Panel e shows that the XRD results are very similar between nanorices and microplates. Panel f shows the schematic of PANI molecular arrangement in a 1D nanorice.

conductivity. Usually, the in-plane electrical charge transport characteristics of the 2D superlattice are strongly affected by three types of disorder (global structural disorder in the array topology; local structural disorder in the interparticle couplings; and local charge disorder, which is due to random immobile charges in the underlying building blocks[52,53]) and proven by the conductivity of the in-plane direction of the microplate. Therefore, although the microplates showed ordered hexagonal topology, the conductivity of its in-plane direction was the lowest. In the normal direction, on the other hand, charge carriers transport along PANI molecule chains but need to overcome the barriers between interchains. Since the intrinsic mobility of intrachain transport should be higher than that of the $\pi-\pi$ sacking direction, the lower conductivity of the normal direction of the nanorice must originate from the high resistance of interchain hopping due to charge carrier traps at the interfaces of neighboring molecules.

In summary, good crystalline nanorices composed of helical PANI molecules and their 2D shoulder to shoulder self-organized hexagonal microplates were obtained by a self-

(52) Kanehara, M.; Kodzuka, E.; Teranishi, T. *J. Am. Chem. Soc.* **2006**, *128*, 13084.
(53) Parthasarathy, R.; Lin, X.; Jaeger, H. M. *Phys. Rev. Lett.* **2001**, *87*, 186807.

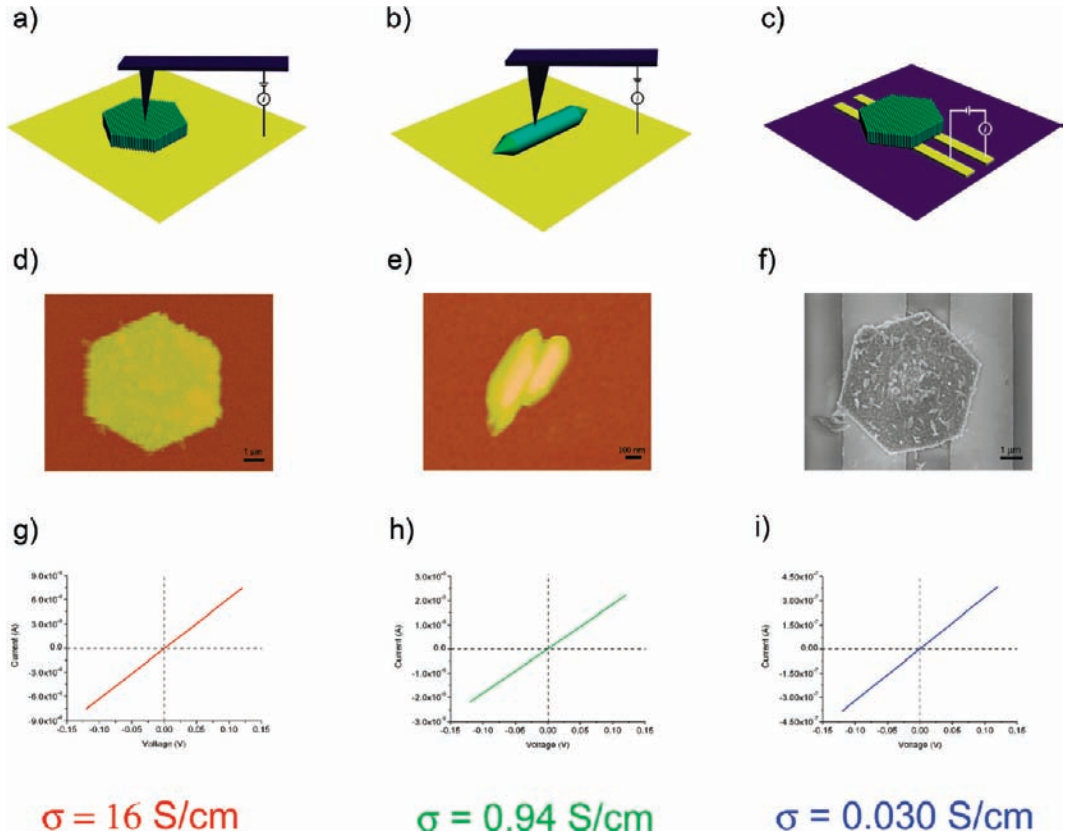

Figure 5. Anisotropic electrical transport character measurements of the ordered hexagonal microplate. Panels a−c show illustrations of electrical measurements in three directions of electrode construction, whereas panel d shows the AFM image. Panel g shows the $I-V$ curve of the microplates shows the highest conductivity. Panel e shows the AFM image, and panel h shows the $I-V$ curve of the nanorice, which has about 1/17 the conductivity of a microplate in the normal direction. Panel f shows the SEM image, and panel i shows the $I-V$ curve of the microplate shows the lowest conductivity due to structural disorder or defects at the interface of neighboring individual nanorices. Both the defects at the interface and low mobility along the main chain direction constitute the anisotropic electrical transportation in microplates.

assembling process. Hexagonal symmetry of the superstructured microplates was a result of the structural hexagonal mesophase due to the helical stacking of PANI molecules. Electrical transport measurements show the anisotropic conductivities of self-assembled microplates and their building blocks. This self-assembly process that produces ordered hexagonal superstructures is made possible by delicately controlling the Brownian motion and the van der Waals forces among PANI molecules and their self-assembled nanostructures. Due to the general principle of the self-assembly process, this strategy could guide further studies on the self-assembly behavior of other chemical and biochemical species.

Acknowledgment. We acknowledge the financial support of the National Natural Science Foundation of China (No. 20974029) and the Ministry of Science and Technology of China (Nos. 2006CB932100 and 2009CB930400). We also appreciate the constructive discussions we had with Prof. M. He, National Center for Nanoscience and Technology regarding our SAED and XRD results.

JA1036447